Instantaneous Flow Reconstruction from Particle Trajectories with Vortex-in-Cell

Schneiders, Jan; Singh, P.; Scarano, Fulvio

Publication date
2016

Document Version
Final published version

Published in
Proceedings of the 18th International Symposium on the Application of Laser and Imaging Techniques to Fluid Mechanics

Citation (APA)
Schneiders, J., Singh, P., & Scarano, F. (2016). Instantaneous Flow Reconstruction from Particle Trajectories with Vortex-in-Cell. In *Proceedings of the 18th International Symposium on the Application of Laser and Imaging Techniques to Fluid Mechanics* Springer.

Important note
To cite this publication, please use the final published version (if applicable).
Please check the document version above.

18TH LISBON 2016
INTERNATIONAL SYMPOSIUM
ON APPLICATIONS OF LASER AND IMAGING TECHNIQUES TO FLUID MECHANICS
FROM 4 TO 7 OF JULY

PROCEEDINGS

OF THE

18th INTERNATIONAL

SYMPOSIUM ON

APPLICATION OF

LASER AND IMAGING

TECHNIQUES TO

FLUID MECHANICS

Instantaneous Flow Reconstruction from Particle Trajectories with Vortex-in-Cell

Jan F.G. Schneiders[1,*], Piyush Singh[1], Fulvio Scarano[1]
1: Dept. of Aerospace Engineering, TU Delft, Delft, The Netherlands
* Correspondent author: J.F.G.Schneiders@tudelft.nl

Keywords: Data Assimilation, VIC+, Particle Tracking Velocimetry, Dense Interpolation

ABSTRACT

The manuscripts presents the working principle of a novel technique to interpolate sparse and scattered particle tracking velocimetry (PTV) measurements onto a dense grid, by using the velocity measurements along a full particle trajectory. The method performs iteratively a vortex-in-cell simulation (Schneiders et al. 2014 in Exp Fluids 55:1692) to minimize the difference between the simulation and the scattered velocity measurements. The optimization is solved using the L-BFGS algorithm where gradients are evaluated efficiently using the adjoint of the vortex-in-cell code. In the numerical assessment, the case of a vortex is considered. At a given seeding concentration, the reconstruction quality of velocity was shown to improve by 50% when a full track is used in comparison to a divergence free reconstruction using only instantaneous velocity. The numerical assessment demonstrates the potential of the method to increase measurement quality and spatial resolution, in comparison to techniques that interpolate velocity using only instantaneous flow information and for example the divergence free constraint.

1. Introduction

The recently introduced VIC+ technique (Schneiders et al. 2015) has been demonstrated to allow for accurate flow reconstruction from time-resolved tomographic PTV experiments at a fraction of the seeding concentrations required for similar accuracy with tomographic PIV, by leveraging the velocity material derivative measured by a particle tracking algorithm. This was called *pouring time into space*. In particular, Schneiders et al. (2015) demonstrated this using the similated experiment along a flat-plate turbulent boundary layer. Furthermore, the method has been utilized in a comparative study, based on a simulated experiment that assesses several methods to obtain pressure from PIV data. The work conducted within the European NIOPLEX consortium (Blinde et al. 2016) showed that the optimization produced with the VIC+ algorithm yields a very accurate reconstruction of the instantaneous pressure field, when compared to other methods based on cross-correlation analysis. The study by Schneiders et al. (2016a) confirmed in the case of a real-world turbulent boundary layer experiment at Re_θ = 2038 that VIC+ can yield more accurate estimates of vorticity magnitude and rms vorticity fluctuations in the boundary layer.

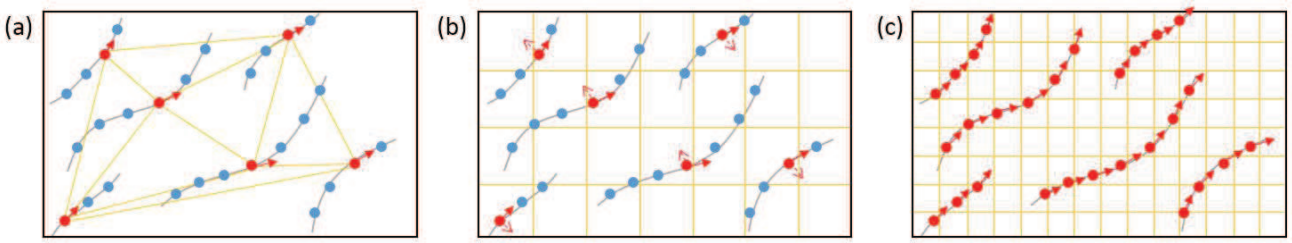

Fig. 1. Schematic of a PTV measurement result. Lagrangian particle trajectory measurements (grey lines) and velocity vectors used for dense velocity reconstruction (red). The tracer particles used for velocity reconstruction are colored red, the others blue. Linear interpolation (a) uses instantaneous velocity only, VIC+ (b) uses also the material derivative and VIC++ (c) uses the full particle trajectory. The yellow lines represent the reconstruction grid.

The VIC+ method uses an iterative gradient-based optimization procedure to incorporate both instantaneous velocity and material derivative measurements into the instantaneous flow reconstruction (Fig. 1b). This is in contrast to techniques that use instantaneous velocity only, such as linear interpolation (Fig. 1a). The use of such iterative reconstruction techniques has received increased attention in literature over the past decade, especially in the field of optical flow (Heitz et al. 2010), but also for example for an investigation in the bottom boundary layer of the coastal ocean measured by submersed tomographic PTV (Vlasenko et al. 2015). For PIV measurements, Gronskis et al. (2013) and Yegavian et al. (2015) use an iterative data-assimilation procedure solving the incompressible Navier-Stokes equations to obtain respectively accurate inflow conditions for later DNS similations and to increase resolution of the PIV measurements. Similarly, Lemke and Sesterhenn (2013) proposed an iterative data assimilation framework using the compressible Navier-Stokes equations for pressure evaluation from PIV measurements. In view of compitational cost, all these methods use an adjoint code to evaluate efficiently the gradients required for the gradient-based optimization. However, still, application of these techniques to real volumetric velocity measurement data has so far however been limited due to competational costs associated with solving the Navier-Stokes equations iteratively on the computational grid.

The iterative optimization frameworks allow for inclusion of more measurement data than, in the case of VIC+, only velocity and its material derivative. Recent advanced in the field of Lagrangian particle tracking algorithms – in particular: Shake-the-Box (Schanz et al. 2016) – have allowed for measurement of long particle trajectories (spanning over > 10 snapshots) in densely seeded flows (comparable to tomographic PIV). This provides accurate and scattered measurements of velocity over time in a measurement volume. The VIC+ method demonstrated increased reconstruction accuracy when velocity and its instantaneous material derivative are

used for reconstruction. When all time-instants are used for reconstruction of the instantaneous flow organization (Fig. 1c), this could allow for increased reconstruction quality of relevant flow quantities, such as rms velocity and vorticity fluctuation levels.

In the present manuscript it is proposed to use full velocity time histories from Lagrangian particle trajectory measurements with the VIC+ framework. The resulting 'VIC++' method requires an extension of the framework to include an iterative time-integration procedure. Because of the computional cost associated with this extension, the focus of the present manuscript is on a concept demonstration on the analytical case of a two-dimensional vortex, to investigate the potential of the method.

2. Pouring Time into Space: Working Principle

The method is based on iterative time-integration using vortex-in-cell (VIC, as applied to PIV measurements in Schneiders et al. 2014). An initial condition is changed at each iteration to minimize the difference between the velocity from VIC time-integration and the PTV velocity measurements (illustrated in Fig. 2). This is a generalization of the VIC+ method proposed earlier in Schneiders et al. (2015), in which time-integration was avoided and only velocity and velocity material derivative is considered for the non-linear iterative optimization. This generalization is called 'VIC++' in the present manuscript.

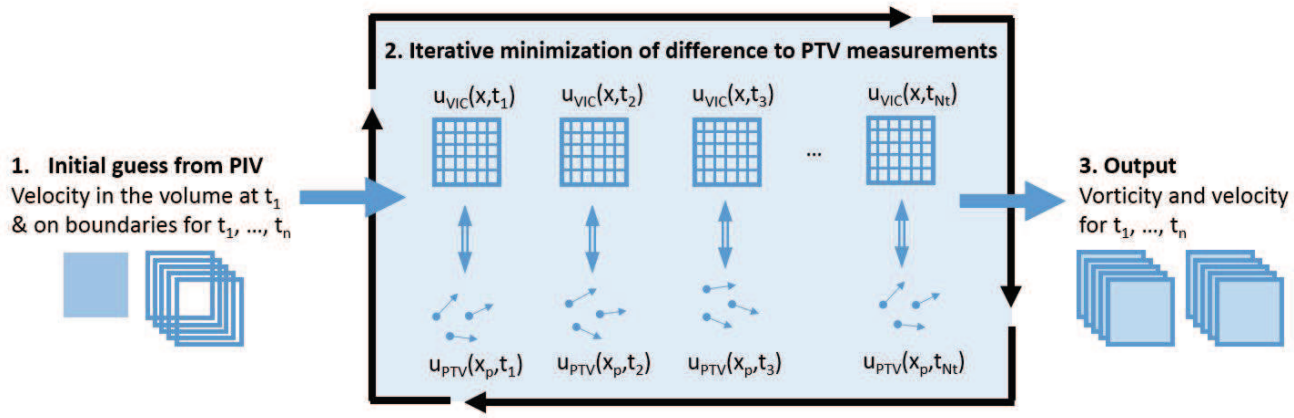

Fig. 2 Flowchart of the proposed velocity reconstruction technique

The method relies on the availability of particle trajectories. This requires time-resolved measurements where particles can be observed moving on long tracks (> 10 snapshots) before exiting the measurement domain. The particle trajectories can be obtained from voxel-based approach (e.g. tomographic PTV) or directly from iterative particle reconstruction (IPR, Wieneke 2014; Shake-the-Box, Schanz et al. 2016).

The matrix containing the locations of all particles at each time-instant is $\overline{\overline{\boldsymbol{X}}}_{\boldsymbol{PTV}}$ of a particle trajectory with length N_t. The corresponding particle velocities are collected in the matrix $\overline{\overline{\boldsymbol{V}}}_{\boldsymbol{PTV}}$. The VIC time-integration starting from an initial condition calculates at each measurement time-instant the velocities $\overline{\overline{\boldsymbol{V}}}_{\boldsymbol{VIC}}$ at the particle locations $\overline{\overline{\boldsymbol{X}}}_{\boldsymbol{PTV}}$. Note the integration time-step dt is typically smaller than the measurement time-interval and determined according to the criteria defined in Schneiders et al. (2014). The computational domain is chosen equal to the measurement volume and linear interpolation is used to obtain $\overline{\overline{\boldsymbol{V}}}_{\boldsymbol{VIC}}$ at $\overline{\overline{\boldsymbol{X}}}_{\boldsymbol{PTV}}$ from the computational grid.

A non-linear optimization problem is defined in which the degrees of freedom (i.e. initial and boundary conditions) are iteratively adjusted to minimize the difference between $\overline{\overline{\boldsymbol{V}}}_{\boldsymbol{VIC}}$ and $\overline{\overline{\boldsymbol{V}}}_{\boldsymbol{PTV}}$ (see Fig. 2, middle). This difference is quantified in the cost function, J, for the optimization procedure,

$$(1) \qquad J = \sum\left[\overline{\overline{\boldsymbol{V}}}_{\boldsymbol{PTV}} - \overline{\overline{\boldsymbol{V}}}_{\boldsymbol{VIC}}\right]^2.$$

A gradient based optimization technique is used (L-BFGS, Liu and Nocedal, 1989) to find the degrees of freedom minimizing the cost function. The degrees of freedom for the optimization are collected in a vector $\boldsymbol{\xi}$. For the gradient based optimization, at each iteration it is necessary to calculate the gradients $dJ/d\boldsymbol{\xi}$. Using finite-differencing, this would come at the cost of the number of degrees of freedom (~ nx×ny×nz) time-integrations *per iteration.* To avoid this, the gradient is calculated efficiently by the numerical adjoint of the VIC code. This is a mathematical 'trick' to evaluate the gradient $dJ/d\boldsymbol{\xi}$ at the CPU cost of a single time-integration only, but at the cost of increased memory usage. The latter memory usage remains however very limited due to the relatively short time-integrations that are performed along particle trajectories of typically 5-20 snapshots. For information on the adjoint, the reader is referred to Talagrand and Courtier (1987), amongst others. The iterative procedure is stopped when the cost function J is on the order of the measurement error in the PTV velocity measurements.

3. Numerical assessment

Consider a two-dimensional Gaussian vortex positioned in the center of a simulated measurement plane. The case of such a vortex blob has been used previously for assessment of time-resolved PIV techniques by amongst others de Kat and van Oudheusden (2012), Lynch and Scarano (2014) and Schneiders et al. (2016b). The tangential velocity field induced by the Gaussian vortex blob is given by,

$$(2) \qquad V_\theta = \frac{\Gamma}{2\pi r}\left(1 - e^{-\frac{r^2}{c_\theta}}\right)$$

where Γ is the circulation and $c_\theta = r_c^2/\gamma$. Choosing $\gamma = 1.256$, the tangential velocity peaks at the core radius r_c. For the present assessment, $\Gamma/V_pL = 1.75$, where Vp is the peak velocity at the core radius r_c. Figure 3a shows the resulting analytical vector field. Figures 3b and c show the u-component of velocity and vorticity, respectively.

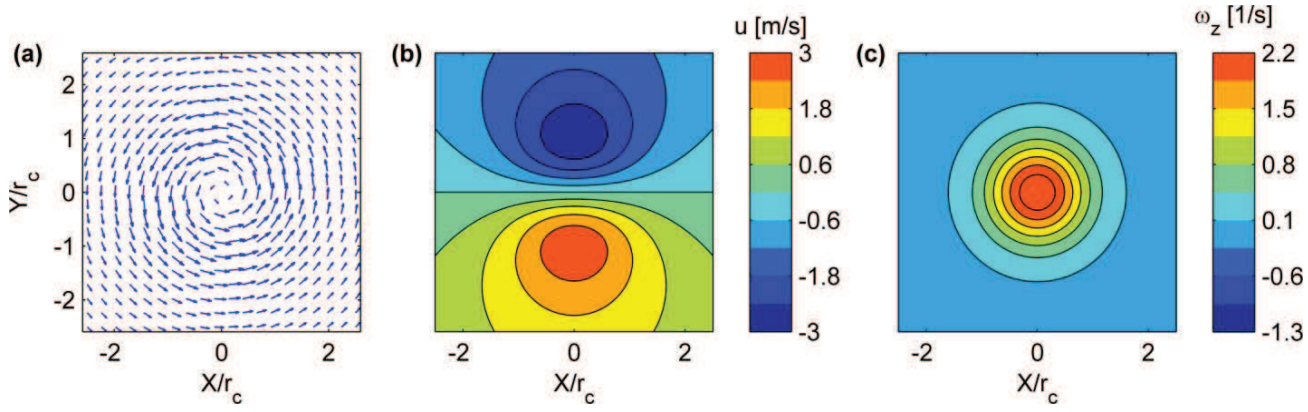

Fig. 3 Reference vector field (a), contours of u velocity (b) and vorticity (c).

The measurement plane is chosen to be a square with sides of $2.5r_c$. Simulated PTV measurements are made by seeding a computational plane uniformly with particles. The particles are integrated over time with the RK4 method, where the instantaneous velocity is provided by the analytical flow field given by (2). Scattered velocity measurements are taken from the analytical flow field at the particle locations at a time-separation of $\Delta t = 0.2$. The total measurement duration is taken to be $N_t = 40$-snapshots. As discussed in the introduction, established techniques to interpolate velocity at t_i from the scattered particle positions onto a dense grid use only the instantaneous velocity measurements t_i. In the present study, trilinear interpolation and adaptive Gaussian windowing (AGW, Agui and Jimenez 1987) are taken as examples of such techniques. The proposed vortex-in-cell technique can also be applied to a single velocity measurement, which results in a divergence free interpolation of the scattered velocity measurements. For all methods, velocity is interpolated to a regular grid with 20 x 20 vectors. For the vortex-in-cell methods, homogeneous padding type boundary conditions (Schneiders et al. 2016b) are employed.

The results are first assessed by comparison of contour plots of instantaneous velocity. Figure 4a shows the instantaneous analytical u-component of velocity. A seeding concentration at which $N_p = 10$ tracer particles are present within at the measurement plane is considered. Figure 4b shows the result of tri-linear interpolation of the scattered velocity measurements to a regular

grid. The instantaneous particle locations are visualized by the red crosses in the figure. The linear interpolation result returns exactly the velocity measurement at the particle locations. In between the measurements, on the other hand, the result is affected by the limited tracer particle concentration and the two concentrated extrema in the velocity field (Fig. 4a) are not found by the linear interpolation (Fig. 4b). The adaptive Gaussian windowing technique returns the weighted averaged velocity field at each grid node, and therefore a filtered result is expected in comparison to the linear interpolation. This is confirmed by the AGW result in Fig. 4c, which is similar to the result of the linear interpolation (Fig. 4b), but shows a reduced velocity gradient.

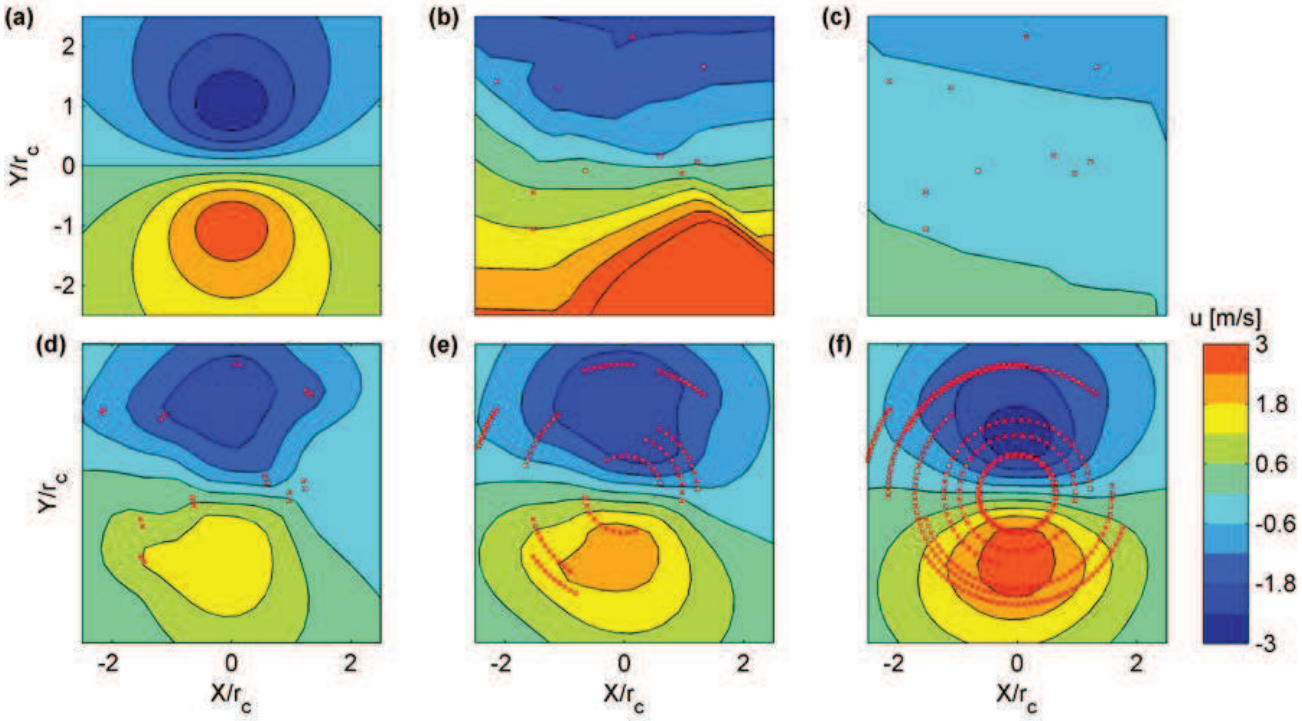

Fig. 4 Contours of the x-component of velocity. Reference flow field (a), linear interpolation (b), AGW (c) and the proposed method with N_t = 2, 10 and 40 (d-f, respectively)

The proposed vortex-in-cell technique can be employed for an instantaneous reconstruction using only one or N_t = 2 velocity measurement, to yield essentially a divergence free reconstruction of the flow. Because this imposes a physics-based restriction on the flow reconstruction, improved accuracy of the velocity reconstruction in between particles is expected. This is confirmed by the result in Fig. 4d, which shows the vortex-in-cell reconstruction using just two velocity time instants (N_t = 2). The result shows the two discrete extrema of u in the reconstruction. When more measurement time-instants are used for the instantaneous velocity reconstruction, a further regularization of the velocity is expected. Figures 4e and f show the results using N_t = 10 and 40 measurement time-instants, respectively. The red

crosses show the particle trajectories over the respective time-durations used for velocity reconstruction. When 40 time-instants are employed, the resulting velocity field is practically symmetric and shows the same contour levels as the reference solution (Fig. 4a). The towards the edges of the domain, the velocity decreases, which is expected as no particles are present in this region.

The results plotted in Fig. 4 depend on the particle locations, in particular for the methods that use only a limited number of time-instants for velocity interpolation. To inspect more closely the differences between short (N_t = *2*) and long (N_t = *40*) track lengths used for velocity reconstruction, Fig. 5a and b show the average profiles along the center line of the measurement plane is given for the u and v components of velocity. The profiles are averaged from multiple random initializations of the particle locations. On average, 10 tracer particles were present in the measurement plane. The analytical profiles are plotted in black. The results for N_t = 2 and 40 are shown in blue and red, respectively. The shaded area represents the standard deviation from the mean results, which represents the variation in the reconstruction quality depending on the particle locations. As expected from the results in Fig. 4, when a longer trajectory is used for reconstruction, the peak velocities are approximated more accurately – at the same seeding concentration.

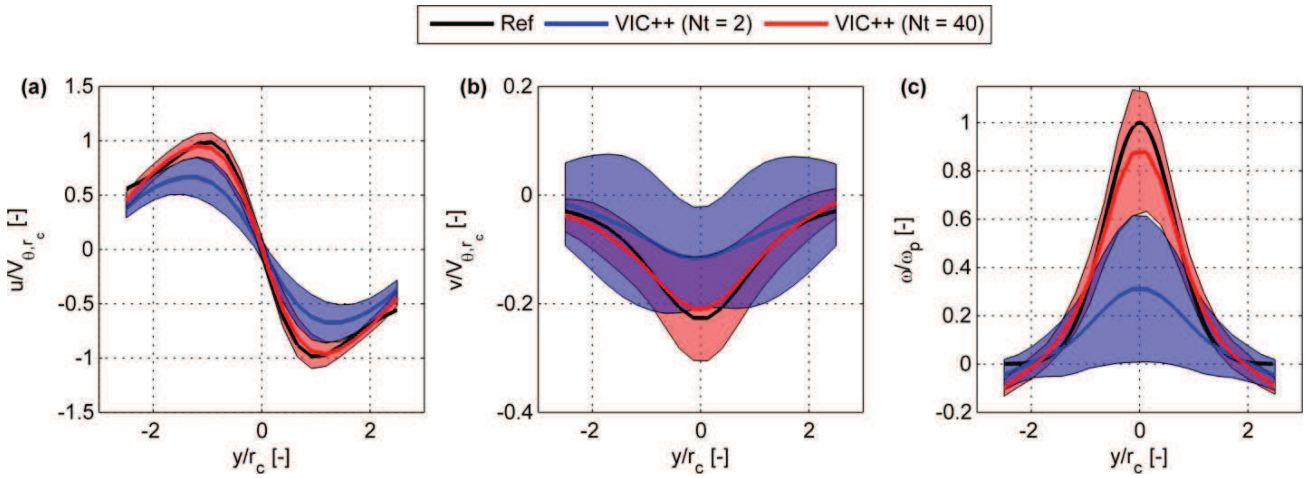

Fig. 5 Average center-line profiles of the velocity components u (a) and v (b) and vorticity (c), calculated from 50 random initializations of the tracer particles.

The improved estimation of the peak velocities when more time-instants are used for reconstruction is expected to yield a more accurate estimation of the peak vorticity levels. The vorticity contour plots are presented in Fig. 6. The figures follow the layout of the velocity contour plots (Fig. 4) discussed above, and again the particles trajectories used for reconstruction are plotted by the red crosses.

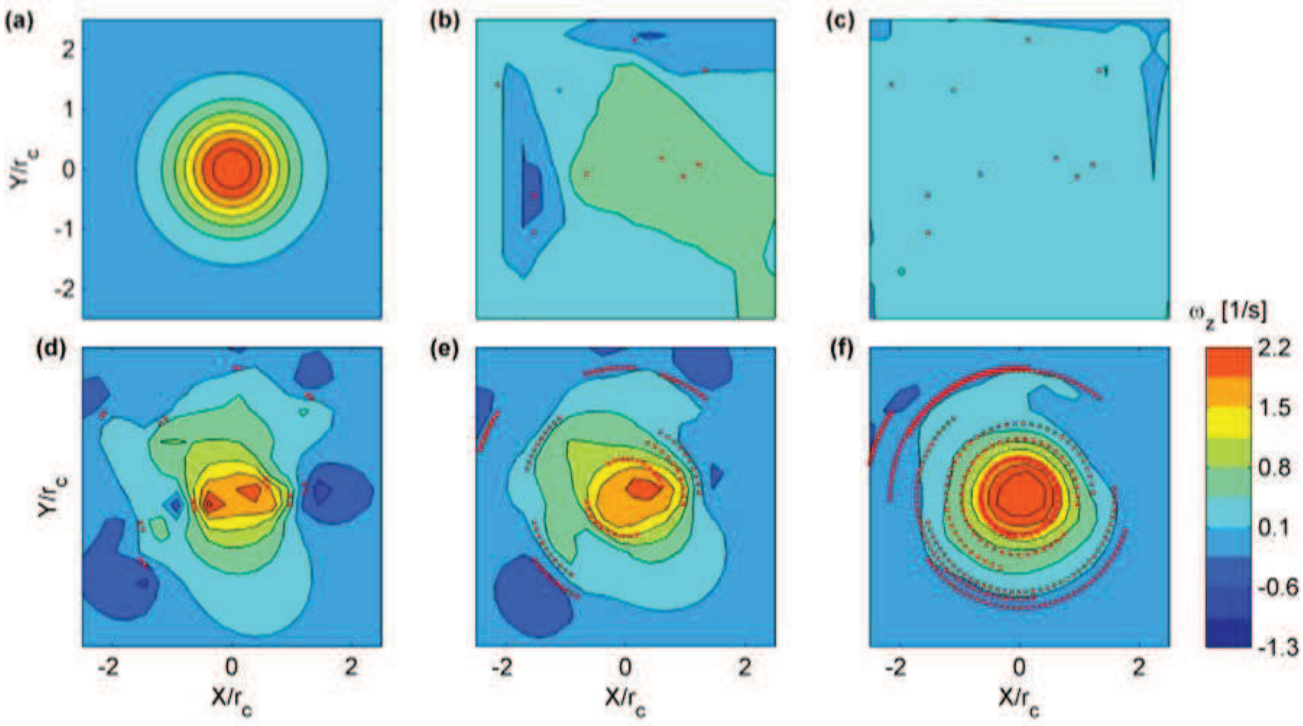

Fig. 6 Contours of vorticity. Reference flow field (a), linear interpolation (b), AGW (c) and the proposed method with Nt = 2, 10 and 40 (d-f, respectively).

As can be expected from the filtered results obtained by the linear interpolation and adaptive Gaussian windowing techniques (Fig. 4b and c, respectively), the vortex blob is not identified by the contours plotted (Fig. 6b and c). The situation is much improved when the divergence free condition is enforced for the reconstruction (Fig. 6d). The shape of the vortex is however affected by the instantaneous particle locations and two peaks are visible in the reconstruction. When more time-instants are used (N_t = 10, Fig. 6e), the result is further regularized and practically circular for N_t = 40 (Fig. 6f). The statistically averaged profiles for vorticity are plotted in Fig. 5c, which confirms that with N_t = 40, the peak vorticity value is better resolved than when essentially only a divergence free reconstruction is made with N_t = 2. It should be remarked that the slight negative vorticity towards the domain boundaries follows from the fixed homogenous velocity boundary conditions used for this assessment.

For a more quantitative comparison of the results, the rms error level of velocity with respect to the analytical solution (eq. 2) is evaluated in the domain center (x, y = $-r_c/2$ to $r_c/2$) and plotted in Fig. 7, which shows the rms error variation with seeding concentration, for the different interpolation techniques considered. The error is normalized by the peak velocity value.

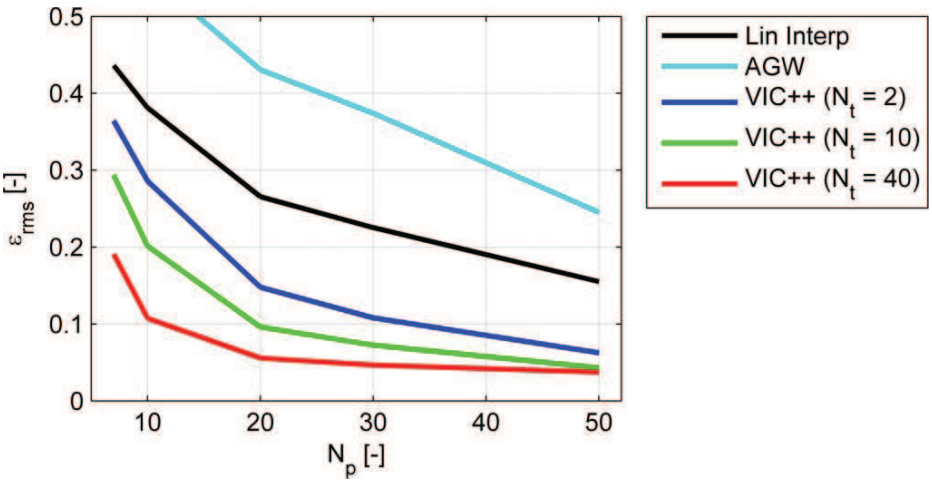

Fig. 7 Velocity rms error variation with number of particles and reconstruction technique.

When the number of particles used for the interpolation increases, the rms error decreases. More noteworthy, for all seeding concentrations, the error decreases when a longer time-series is used for the VIC++ reconstruction. The flattening of the N_t = 40 result for large Np is ascribed to the finite and relatively coarse grid size used for the reconstruction. This shows the potential of the novel technique to improve velocity accuracy in cases where time-resolved measurements are available.

4. Conclusions

The novel concept of using full particle trajectory measurements with vortex-in-cell simulations to allow for a dense interpolation of velocity in the measurement region is outlined and demonstrated on the numerical case of vortex blob. For all seeding concentrations considered, the use of longer particle trajectories yields a more accurate reconstruction of the velocity field. The study demonstrates the potential of assimilation of long Lagrangian particle trajectory measurements (e.g. from tomographic PTV or "Shake-the-Box") with vortex-in-cell simulations for increased accuracy of velocity and vorticity measurements.

Acknowledgements

This research is partly funded by LaVision GmbH.

References

Agui and Jimenez 1987

Blinde P, Michaelis, D., van Oudheusden, B. W., Weiss, P.-E., de Kat, R., Laskari, A., Jeon, Y. J., David, L., Schanz, D., Huhn, F., Gesemann, S., Novara, M., McPhaden, C., Neeteson, N., Rival, D., Schneiders, J. F. G., Schrijer, F. (2016) Comparative assessment of PIV-based pressure evaluation techniques applied to a transonic base

flow. In: 18th international symposium on the application of laser techniques to fluid mechanics. Lisbon, Portugal. 4-7 July.

de Kat, R., & van Oudheusden, B. W. (2012) Instantaneous planar pressure determination from PIV in turbulent flow. Experiments in Fluids, 52, 1089–1106.

Gronskis, A., Heitz, D., & Mémin, E. (2013) Inflow and initial conditions for direct numerical simulation based on adjoint data assimilation. J Comput Phys 242, 480–497.

Heitz, D., Memin, E., & Schnorr, C. (2010) Variational fluid flow measurements from image sequences: synopsis and perspectives, Experiments in Fluids, 48, 369-393

Lemke, M., & Sesterhenn, J. (2013) Adjoint based pressure determination from PIV-data—validation with synthetic PIV measurements. In: 10th international symposium on PIV, Delft, The Netherlands.

Lynch, K., & Scarano, F. (2014) Material acceleration estimation by four-pulse tomo-PIV. Meas Sci Technol 25:084005

Schanz, D., Gesemann, S., & Schröder, A. (2016). Shake-The-Box: Lagrangian particle tracking at high particle image densities. Experiments in fluids, 57, 70.

Schneiders, J. F. G., Dwight, R. P., & Scarano, F. (2014). Time-supersampling of 3D-PIV measurements with vortex-in-cell simulation. Experiments in Fluids, 55, 1692.

Schneiders, J. F. G., Azijli, I., Scarano, F., & Dwight, R. P. (2015). Pouring time into space. In: 11th International Symposium on Particle Image Velocimetry, PIV15, Santa Barbara, CA, USA, September 14-16 2015.

Schneiders, J. F. G., Scarano, F., Elsinga, G. E. (2016a) On the Resolved Scales in a Turbulent Boundary Layer by Tomographic PIV and PTV aided by VIC+. In: 18th international symposium on the application of laser techniques to fluid mechanics. Lisbon, Portugal. 4-7 July.

Schneiders, J. F. G., Pröbsting, S., Dwight, R. P., van Oudheusden, B.W., & Scarano, F. (2016b). Pressure estimation from single-snapshot tomographic PIV in a turbulent boundary layer. Experiments in Fluids, 57, 53.

Vlasenko, A., Steele, E. C. C., Nimmo-Smith, W. A. M. (2015) A physics-enabled flow restoration algorithm for sparse PIV and PTV measurements. Meas Sci Technol 2015:065301

Yegavian, R., Leclaire, B., Champagnat, F., & Marquet, O. (2015) Performance assessment of PIV super-resolution with adjoint-based data assimilation. In: 11th international symposium on PIV, Santa Barabara, CA, USA, September 14-16 2015.

Wieneke, B. (2014) Iterative reconstruction of volumetric particle distribution. Measurement Science and Technology, 24, 024008.